Rony Caballero

Technological University of Panama
Apartado Postal 622894
El Dorado, Panama City, Panama

Manuel A. Armada
Teodor Akinfiev

Automatic Control Department
Industrial Automation Institute – CSIC
28500 La Poveda, Madrid, Spain
armada@iai.csic.es

Robust Cascade Controller for Nonlinearly Actuated Biped Robots: Experimental Evaluation

Abstract

In this paper we consider the postural stability problem for nonlinearly actuated quasi-static biped robots, both with respect to the joint angular positions and also with reference to the gripping effect between the foot/feet against the ground during robot locomotion. Zero moment point based mathematical models are developed to establish a relationship between the robot state variables and the stability margin of the foot (feet) contact surface and the supporting ground. Then, in correspondence with the developed dynamical model and its associated uncertainty, and in the presence of non-modeled robot mechanical structure vibration modes, we propose a robust control architecture that uses two cascade regulators. The overall robust control system consists of a nonlinear robust variable structure controller in an inner feedback loop for joint trajectory tracking, and an $\mathcal{H}_\infty$ linear robust regulator in an outer, direct zero moment point feedback loop to ensure the foot–ground contact stability. The effectiveness of this cascade controller is evaluated using a simplified prototype of a nonlinearly actuated biped robot in double support placed on top of a one-degree-of-freedom mobile platform and subjected to external disturbances. The achieved experimental results have revealed that the simplified prototype is successfully stabilized.

KEY WORDS—biped robots, stability, zero moment point, robust control, nonlinear control, nonlinear actuators

1. Nomenclature

1.1. General Notation

$q =$ Joint angular position vector
$\dot{q} =$ Joint angular velocity vector
$\ddot{q} =$ Joint angular acceleration vector

The International Journal of Robotics Research
Vol. 23, No. 10–11, October–November 2004, pp. 1075-1095,
DOI: 10.1177/0278364904047394

$\theta_i =$ Angle of link$_i$ against vertical
$q_i =$ Relative angle between link$_i$ and link$_{i-1}$

1.2. Actuator Dynamic Modeling

$\gamma_i =$ Motor axis angle (input angle for joint$_i$)
$\dot{\gamma}_i =$ Motor axis speed (input speed for joint$_i$)
$\ddot{\gamma}_i =$ Motor axis acceleration (input acceleration for joint$_i$)
$A_{vi} =$ Nonlinear transmission ratio for joint$_i$
$U =$ Feeding voltage in motor terminals
$\Psi =$ Nonlinear matrix accounting for inertial effects
$\Phi =$ Nonlinear matrix accounting for damping and Coriolis effects
$\Upsilon =$ Nonlinear matrix accounting for quadratic speed effects caused by the nonlinear transmission
$\Delta =$ Nonlinear vector accounting for gravity and other nonlinear effects

1.3. Control

$s =$ Laplace transform
$\omega =$ Frequency (rad s^{-1})
$\varphi(t) =$ Sliding surface function
$P(s) =$ Plant transfer function
$\Delta(s) =$ Plant uncertainty transfer function
$S_p =$ Sensitivity function
$T_p =$ Complementary sensitivity function
$G_i =$ Nominal transfer function (i)
$C_i =$ Controller transfer function (i)
$F_i =$ Feedforward compensator transfer function (i)

2. Introduction

The biped robot stabilization problem is an active field of investigation. Researchers such as Vukobratovic and Juricic

(1968, 1969), Hemami, Weimer, and Koozekanani (1973), Vukobratovic et al. (1990), and Goswami (1999) have presented relevant contributions regarding models and stability indexes that allow us to analyze and to understand the underlying physical aspects of such a problem. Nevertheless, the usefulness of the available models is sometimes limited in practice by their inherent complexity and by the always existing uncertainties in practical realizations.

In order to provide a comprehensible framework of the present research activities in this field of biped robot control, and to position in a proper way the contributions of this paper, it is convenient to recall here that biped robots can be broken up into two major groups: dynamic or ballistic biped robots, and quasi-static biped robots. Dynamic biped robots are usually designed for trotting or running and present dynamic stability properties (Furushu and Masubushi 1986; McGeer 1990; Seo and Yon 1995; Waldron 2000). Quasi-static biped robots are designed for walking, with the main difference from dynamic biped robots being the use of feet to help them to stand statically (Takanishi et al. 1989; Eldukhri 1996; Fujimoto, Obata, and Kawamura 1998; Hirai 1999).

One relevant aspect in present biped robot research is the selection of efficient joint actuators (Medrando-Cerda and Eldukhri 1997). As pointed out by many authors (Pratt, Dilworth, and Pratt 1997; Sardin, Rostami, and Besonet 1998; Pfeiffer, Löffler, and Gienger 2000), the solution to this problem is still an active area of investigation. Interesting proposals for biped robot actuation comprise from passive dynamics (McGeer 1990) to resonance drives (Akinfiev 1996), and include artificial muscles (Mennitto and Buehler 1997; Yamaguchi and Takanishi 1997) and special actuators (Pratt, Dilworth, and Pratt 1997).

On the other hand, it is well known that one of the most effective ways to analyze the stability of biped robots is the so-called zero moment point (ZMP), introduced by Vukobratovic and Stokic (1975), to be used as an index of stability for the walking cycle. The ZMP can be considered as an extension of the center of mass projection (Hemami 1978; Sias and Zheng 1987), and has been employed successfully by many authors for biped robot trajectory selection (Takanishi et al. 1989; Yamaguchi, Takanishi, and Kato 1993; Fujimoto, Obata, and Kawamura 1998; Hirai et al. 1998). Very recently, an overview concerning the relevance of the ZMP has been published by the leading investigator (Vukobratovic and Borovac 2004).

In this paper we consider the postural stability problem for nonlinearly actuated quasi-static biped robots, both with respect to the joint angular positions and also with reference to the gripping effect between the foot (feet) against the ground during the robot locomotion. ZMP-based mathematical models are developed to establish a relationship between positions, speeds, and accelerations of the robot joints and the stability margin of the "free joint" between the foot (feet) contact surface and the supporting ground. Then, in correspondence with the developed dynamical model and its associated uncertainty, and in the presence of non-modeled robot mechanical structure vibration modes, we propose a robust control architecture that uses two cascade regulators. The first regulator (inner feedback loop) consists of a nonlinear variable structure controller (VSC) synthesized by using the direct Lyapunov method; it is intended to minimize the trajectory tracking errors at joint level by acting directly on the motors feeding voltage. The second regulator (outer feedback loop) consists of a robust linear controller synthesized by using $\mathcal{H}_\infty$ techniques, with the goal being to guarantee the robot stability (in single support or in double support) by acting on the set points of the first regulator.

The effectiveness of this cascade controller is evaluated using a simplified prototype of a nonlinearly actuated biped robot in double support placed on top of a one-degree-of-freedom mobile platform and subjected to external disturbances. The achieved experimental results, shown afterwards in the final part of the paper, reveal clearly that the simplified prototype is successfully stabilized against both direct ZMP and platform disturbances, thus confirming the practical usefulness of the proposed approach. Finally, we show how the addition of a feedforward term to the cascade controller can help to improve the system response.

3. Nonlinearly Actuated Biped Robots

DC servos with constant transmission ratio are one of the most common choices for driving walking robots (Hirosi et al. 1991; González de Santos, Armada, and Jiménez 2000; Armada et al. 2003b). Nevertheless, when using this classical approach, it is well known that there are hitherto some practical realization problems due to technological limitations posed by the available actuators, which means that, currently, the overall performance of walking robots is far from being optimal. It should be taken into consideration that the torque delivered by the motor must compensate not only for the friction and for the inertial effects, but also for the gravitational effect. The gravitational effect is highly dependent on the joint angle values (the robot configuration changes along the gait). These effects can be compensated using small power motors with high constant transmission ratios, but this approach has the disadvantage of limiting joint velocities. This means that, for example, for a biped robot, at some gait instants, it may happen that we do not have enough "resources" for stabilization. One possible solution to confront such a situation could be to use high power motors with low constant transmission ratios. However, then the weight and thus the global power consumption of the robot are increased, leading to design problems. So, we are pressed to deal with the search, in general terms, for more efficient actuators or, what is more important, for actuators more adapted to the specific features of locomotion. On the other hand, it has been established that nonlinear transmission ratio actuators could improve mechanical design and decrease energy consumption in many

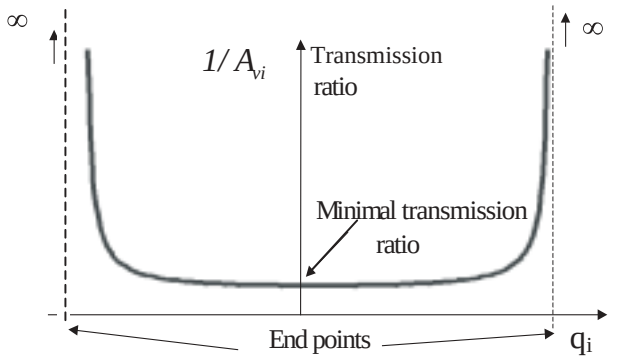

Fig. 1. Nonlinear transmission ratio function provided by SMART.

mechanical systems (Van de Straete and Schutter 1999). The search for efficient locomotion mechanisms for walking machines (and, in particular, for biped robots) has yielded to the creation of the SMART (Special Mechatronic Actuator for Robot joinTs) drive (Akinfiev, Armada, and Caballero 2000; Caballero et al. 2001), which provides a variable reduction ratio and has been considered for use as an efficient actuator for humanoid robots (Caballero et al. 2002a). This drive is characterized by the change of the reduction ratio (transmission ratio, *tr*) from some value in the medium part of a trajectory (e.g., 2.5) *ad infinitum* at its end positions (Figure 1). It has been implemented by using a four-bar linkage mechanism, where all of the individual links are of different lengths. More precisely, the four-bar linkage is made up of two real rods, rod and crank, and two virtual rods (Figure 2). Moreover, it has been demonstrated that the nonlinear transmission is more efficient than the classical constant transmission, and saving of power expenditure could reach up to 75% compared with the classical design (Caballero et al. 2001). Such claimed energy saving is, of course, of major relevance if we are aiming to extend walking robot functioning (Armada et al. 2003a). An in-depth description of SMART advantages has been published recently (Montes et al. 2004). On the other hand, it has been shown that this actuator shares some properties of the highly efficient quasi-resonance drives, but presents the added difficulty of a nonlinear dynamic regime that should be taken into account when designing robot control algorithms (Caballero 2002). So, when trying to use the mechanical advantage provided by the SMART nonlinear actuator, we will need to pay for extra complexity on the control side.

The nonlinear mechanical transmission function (Akinfiev, Armada, and Caballero 2000) (shown in Figure 1), which relates the output joint angle, q_i, with the input angle, γ_i (Figure 2), can be approximated in practice in a compact form given by

$$tr(q_i) = \frac{g(q_{0_i})}{q_{0_i}\sqrt{1 - \frac{q_i^2}{q_{0_i}^2} f^2(q_i)}}$$

for

$$\begin{aligned} & -q_{0_i} \le q_i \le q_{0_i} \\ & 1 - |\xi| \le f(q_i) \le 1 + |\xi| \\ & (1 - |\zeta|)k \le g(q_i) \le (1 + |\zeta|)k \\ & |\xi| \ll 1 \qquad\qquad |\zeta| \ll 1 \end{aligned} \tag{1}$$

where the end points of the SMART actuator output angle (that is the boundaries for its angular span $[-q_{0i}, q_{0i}]$) are determined by the length of the SMART rods (Figure 2). Please note that sometimes it is more convenient to use the inverse of $tr(q_i)$, $1/A_{vi}(A_{vi=}q_i/\gamma_i)$, as shown in Figure 1. The corresponding relationships for the accelerations have been worked out. For a more detailed analysis of the SMART actuator, please refer to Caballero (2002) and Montes et al. (2004).

So, according to the previous statements and referenced investigations, it can be said that using nonlinear transmissions allows us to exploit much better the special characteristics of biped locomotion (Caballero et al. 2001; Montes et al. 2004), where maximum torque and maximum speed do not occur simultaneously for most joints along the walking cycle (Winter 1990).

In order to fully validate the use of nonlinear actuators for biped locomotion, the SILO2 humanoid robot was designed at the Industrial Automation Institute (IAI-CSIC) with an initial number of 23 degrees of freedom. This design considers two degrees of freedom in each ankle, one in each knee, three in each hip, two in the trunk, three in each arm, and three in the head with stereo vision (Armada et al. 2002). This humanoid robot has two different types of actuators: classical and nonlinear actuators. Nonlinear actuators drive two ankle joints in the sagittal plane, two knee joints in the sagittal plane, and two hip joints in the lateral plane. The mechanical configuration of SILO2 is shown in Figure 2, along with a detailed view (right side) of one of the six SMART drives it incorporates (the ankle one in this case). We can see the "four-bar" linkage mechanism that makes the nonlinear transmission from the input angle γ (provided by the input DC motor) to the output angle q (ankle joint in this case), accordingly with (1). SILO2 humanoid robot weights 60 Kg and measures 1.55 m. The control experiments reported here in this paper has been performed with a first, simplified prototype of this machine, working on the sagittal plane, as it will be shown in what follows.

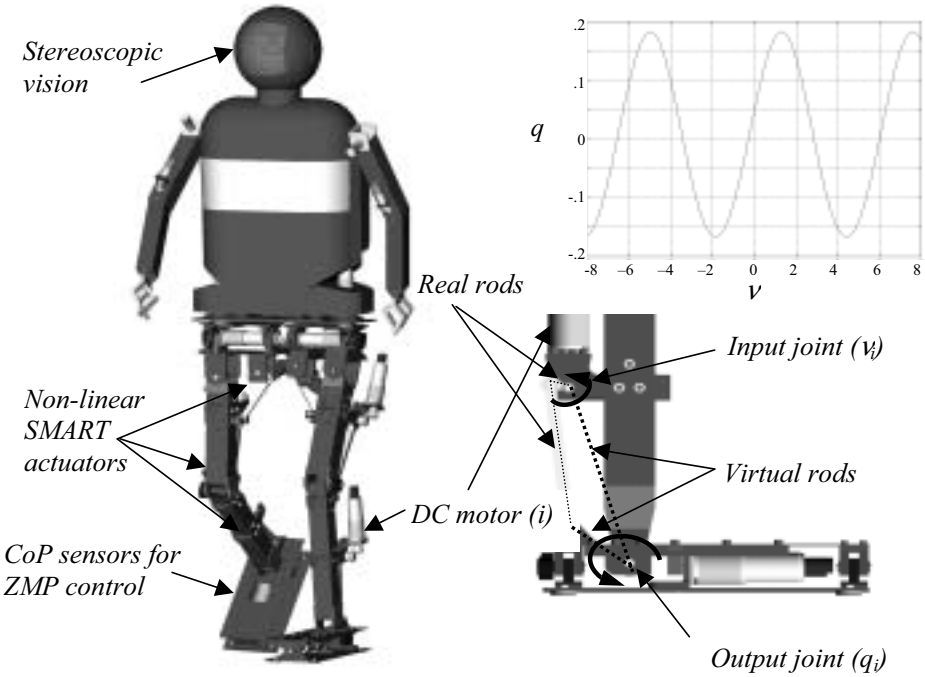

Fig. 2. SILO2 humanoid robot incorporates at lower limbs: six SMART nonlinear actuators (saggital ankle, knee, abduction), and six classical, constant transmission ratio actuators (lateral ankle, lateral hip, saggital hip). The nonlinear relationship between input angle γ and output angle q is also shown.

4. Reduced-Order Models for Quasi-Static Biped Robot Control

One of the major problems in quasi-static biped robot control is during the single-support phase. During this walking phase, the robot is supported only on one foot and so it is more difficult for it to cope with disturbances. Some disturbances, like those of impulse type, can originate discontinuities on the joint speeds, which are translated into tracking errors, or, in the worst case, in losing walking cycle stability, and these are frequently also followed by the robot tripping over. However, if the control system is robust enough, the existing joint tracking errors can be damped very fast and the robot will tend to stabilize, although the disturbances take it momentarily off the foot support.

One way of studying the disturbance effect is by enlarging the robot dynamic equations, adding an extra passive joint connected with the ground. In this sense, the inverted pendulum is a very useful model for single-support stability investigation and has been proposed by Hemami, Weimer, and Koozekanani (1973); see Figure 3. When the robot potential energy is much greater than its kinetic energy, an inverted pendulum can approximate the robot with a passive joint between the foot and the ground.

As mentioned previously, the ZMP is very useful for studying the stability of biped robots. However, the use of a full

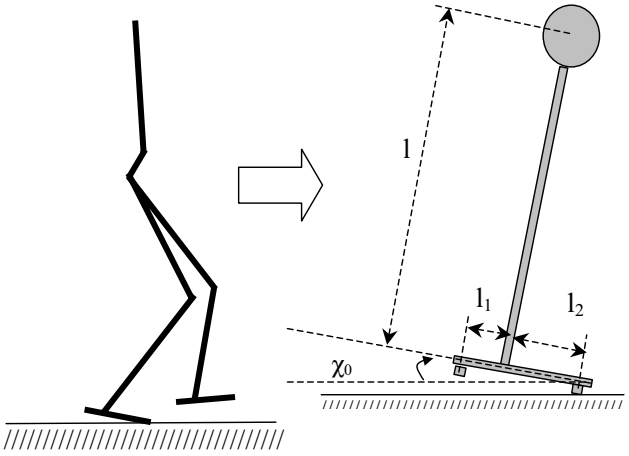

Fig. 3. Inverted pendulum model with a supporting foot.

mathematical model for the ZMP calculation yields complex equations in the form of $ZMP = f(q, \dot{q}, \ddot{q})$, which poses limitations for real-time trajectory planning and/or for being used in designing ZMP-based control systems. One way to overcome the ZMP model complexity could be to use a simplified (reduced-order) model incorporating a limited parametric uncertainty instead of the full biped robot model, and then to

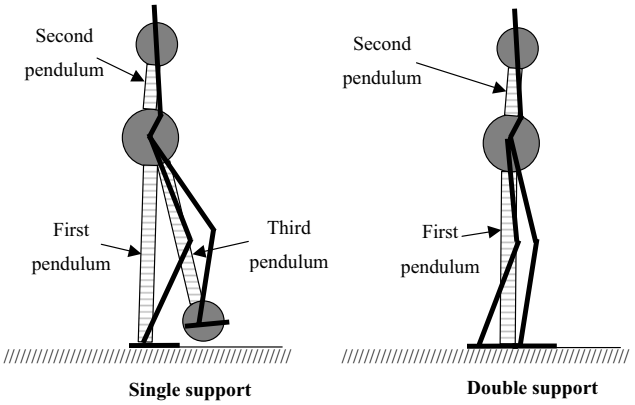

Fig. 4. Reduced-order models for biped robot control.

observe its effect on the ZMP values. The use of reduced-order models in biped robot control is not new, but generally they are employed only for qualitative purposes. Here it is proposed to adjust the complete biped robot model by three coupled inverted pendulums for the single-support phase, and by two inverted pendulums for the double-support phase (see Figure 4).

In our particular case we have an added problem: the use of nonlinear actuators. It can be demonstrated (Caballero, Akinfiev, and Armada 2002b) that, by including the nonlinear actuators in the ZMP model, a new model, more complex, can be obtained. As an example, for the single-support phase, the ZMP is given by

$$ZMP(t) = \alpha_0 + \alpha_1\gamma - \alpha_2\dot{\gamma}^2 - \alpha_3\ddot{\gamma}. \qquad (2)$$

The model given by eq. (2) and illustrated by the block diagram of Figure 5 is a nonlinear system model, but it still considers the robot as a sequence of rigid links actuated by ideal driving units, without taking into account link flexibilities, backlash, saturation effects, and/or modeling errors. One way to improve the previous model is to use a model which incorporates the uncertainty, as shown in Figure 6, where the block P represents the input/output nominal model for α_0 and γ giving ZMP as output, and ΔP represents the model uncertainty due to link flexibility, backlash and other non-modeled mechanical effects.

5. Overall Robust Cascade Control System Architecture

The design of a control system for a biped robot is indeed a complex problem that has received the attention of many researchers. Some contributions to solving this problem propose the use of multivariable control techniques (Mita et al. 1984; Furushu and Sano 1990; Medrano-Cerda and Eldukhri 1997), the use of feedback linearization (Fujimoto, Obata, and Kawamura 1998; Gienger, Löffler, and Pfeiffer 1999), or the use of variable structure control (Raibert, Tzafestas, and Tzafestas 1993; Tzafestas, Krikochoritis, and Tzafestas 1997).

The right determination of the most appropriated solution for the control of a biped robot depends on many factors including the following.

- The degree of dynamical model nonlinearity. If the system is quasi-linear then it becomes more natural to use linear system techniques. This is the situation for a biped robot actuated by classical driving units and performing quasi-static locomotion.
- The degree of coupling among the state variables. If coupling is weak, then it could be enough to use local (single) joint control techniques. This may happen when the transmission ratios are very high and/or when the driving motors are of very high power compared with that actually demanded by the load.
- The uncertainty degree of the system. It is straightforward that if the uncertainty is very high, it will lead to the use of robust control techniques.
- The zero dynamics stability. Zero dynamics can be understood as an extension of the pole placement problem for linear systems to nonlinear systems. It is well known that if the system has a zero on the right half-plane, it is not easy to control.

The first step towards the control architecture selection is to introduce eq. (2) in the classical dynamic model of the biped robot (Caballero 2002). Doing so, a new model incorporating the nonlinear actuators is obtained, as illustrated in Figure 7.

It is clear that the resulting model is nonlinear and in addition it presents a non-minimal phase characteristic. To control such a system, it is suitable to select a cascade control structure (Skogestad and Postlethwaite 1996); see Figure 8.

The cascade control structure is characterized by having two feedback loops. The inner loop regulator, K_2, has the mission of compensating both the disturbances d_2, and the nonlinearities of G_2, while the outer loop regulator, K_1, should compensate the disturbance d_1, and also must operate on G_1, that has non-minimum phase behavior.

However, the use of a classical linear cascade controller could be not enough for the quasi-static control of a biped robot driven by nonlinear actuators (such as SMART, for example), due to the system high degree of nonlinearity. So, we have proposed (Caballero, Akinfiev, and Armada 2002b) the robust cascade architecture shown in Figure 9, characterized by employing a robust nonlinear variable structure controller in the inner loop, and by a robust linear controller synthesized by means of $\mathcal{H}_\infty$ techniques in the outer feedback loop. The inner controller is designed for obtaining a very fast time response, and it is in charge of controlling position γ and speed

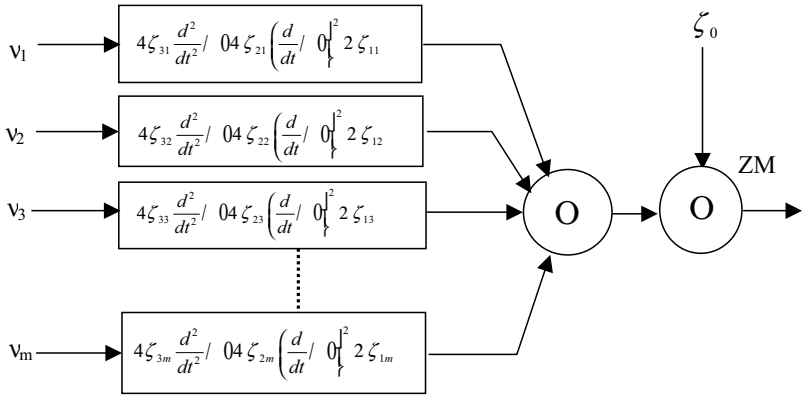

Fig. 5. Single-support ZMP model for a biped robot including nonlinear actuators.

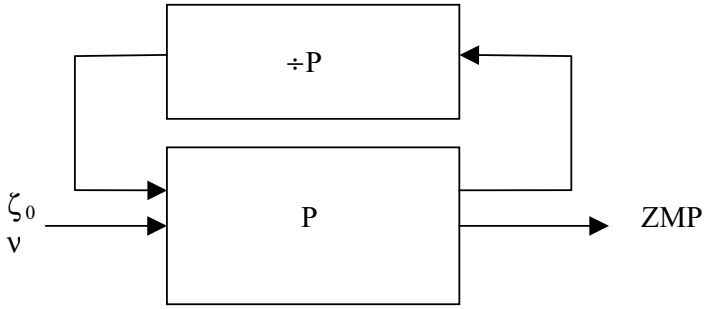

Fig. 6. Single-support ZMP model incorporating system uncertainties.

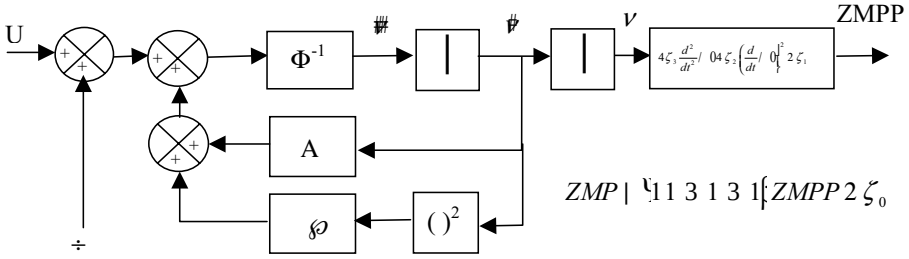

Fig. 7. Full-order dynamical model of the nonlinearly actuated biped robot.

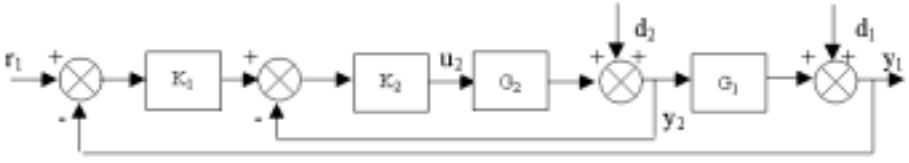

Fig. 8. Classical cascade control block diagram.

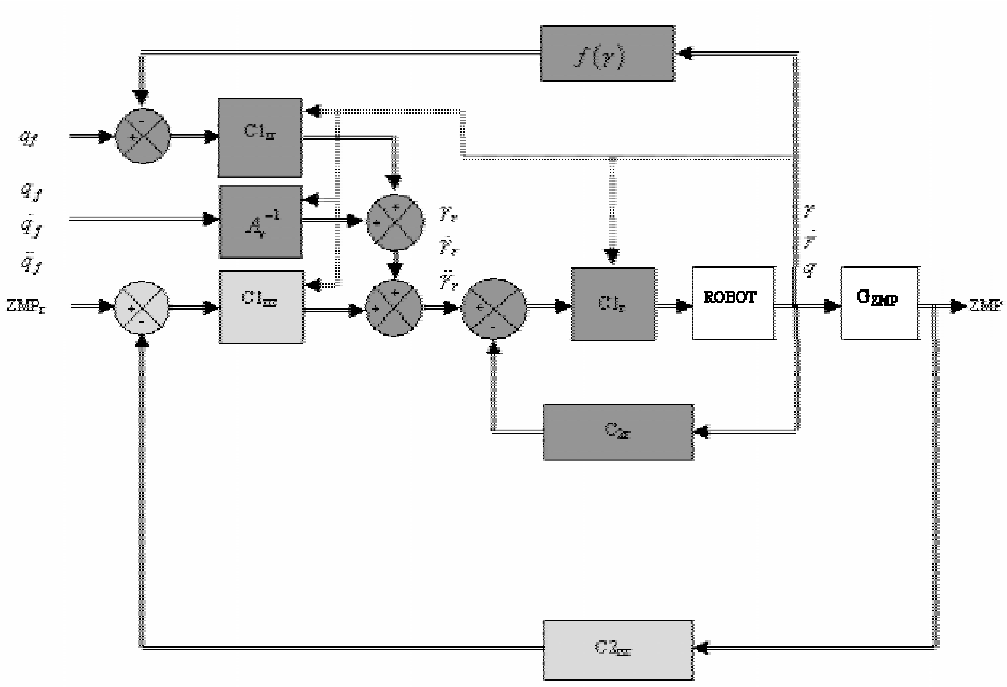

Fig. 9. Proposed cascade control architecture for nonlinearly actuated quasi-static biped robot stance stability.

of the input $\dot{\gamma}$ (driving) motors, controlling also indirectly the position q and the speed $\dot{q}$ of the robot joints. The outer controller is in charge of guaranteeing the stability along the locomotion cycle, and to do so it establishes changes on the set points for the angular position γ and speed $\dot{\gamma}$ of the motor axis.

6. Inner loop Variable Structure Controller Design

The equivalent biped robot dynamical model can be expressed as

$$\Psi(\gamma)\ddot{\gamma} + \Phi(\gamma)\dot{\gamma} + \Upsilon(\gamma)\dot{\gamma}^2 + \Delta(\gamma) = U \tag{3}$$

where γ is the angle of the driving DC motor axis, Ψ is the equivalent inertia matrix, Φ is a damping matrix, Υ is a matrix that considers some quadratic nonlinearities, Δ is a nonlinear vector, and U is the equivalent torque control vector.

Using the direct Lyapunov method, it can be demonstrated (Caballero 2002) that the following robust nonlinear VSC regulator stabilizes the dynamical system given by eq. (3)

$$U = \hat{U} + U_n \tag{4}$$

where

$$\hat{U} = \hat{\Psi}\ddot{\gamma}_{rx} + \hat{\Phi}\dot{\gamma}_{rx} + \hat{\Upsilon}\dot{\gamma}_{rx}^2 + \hat{\Delta} \tag{5}$$

$$U_n = -K_I s - K_s v(s) \tag{6}$$

$$v_i(s_i) = \begin{cases} \frac{s_i}{\|s_i\|} & \text{for } \|s_i\| \geq s_{ai} > 0 \\ \frac{s_i}{s_{ai}} & \text{for } \|s_i\| < s_{ai} \end{cases} \tag{7}$$

$$s = \dot{\gamma} - \dot{\gamma}_r + \Lambda\gamma - \Lambda\gamma_r. \tag{8}$$

The meaning of the other symbols used is as follows: $\hat{\Psi}$, estimated inertia matrix; $\hat{\Phi}$, estimated damping matrix; $\hat{\Upsilon}$, estimated quadratic damping matrix; $\hat{\Delta}$ estimated nonlinear vector; Λ, positive definite diagonal matrix; $\dot{\gamma}_{rx}$, reference velocity; $\ddot{\gamma}_{rx}$ reference acceleration; K_I and K_s, positive definite constant matrices.

Figure 10 illustrates the VSC controller. This regulator has the advantage of avoiding the inversion of the biped robot equivalent highly nonlinear inertia matrix.

7. Outer Loop Linear Robust Controller Design

In order to close the abovementioned second feedback loop, it is necessary to follow the next main steps.

(a) ZMP modeling for direct feedback control. This will be done experimentally for the simplified prototype using frequency response techniques.

(b) $\mathcal{H}_\infty$ linear robust control synthesis.

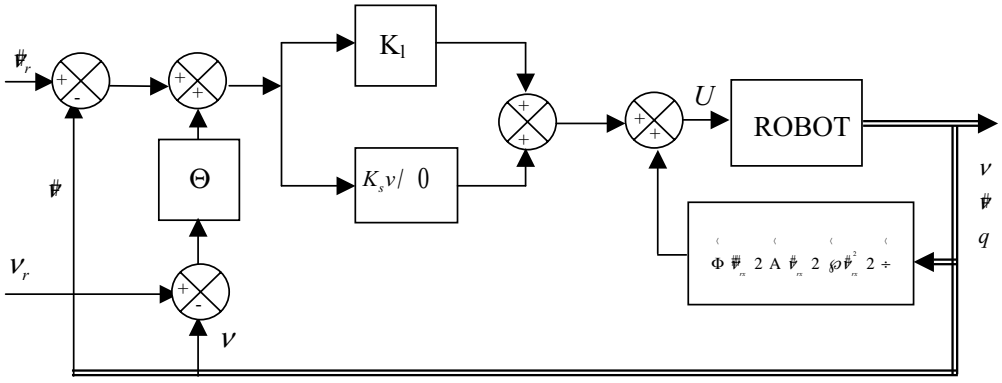

Fig. 10. Robust VSC nonlinear controller for SILO2 robot joints.

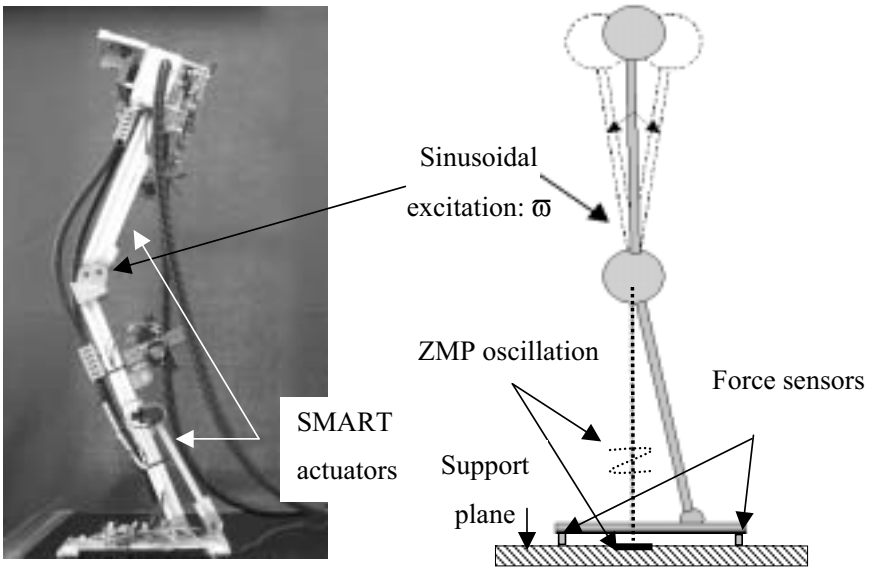

Fig. 11. Two-degrees-of-freedom prototype. ZMP frequency domain model estimation using harmonic oscillations.

After these stages have been accomplished, then the practical implementation of the full cascade controller and the experimentation to test the system properties will be performed.

7.1. ZMP Modeling

In order to obtain a nominal frequency response model for the ZMP, considering its characteristic uncertainty, about any operating point, the upper degree of freedom of a simplified double-support biped robot prototype (actuated by one SMART) is excited with a variable frequency sinusoidal signal (see Figure 11, right side "simplified", not showing the SMART actuator, which can be seen in the photograph for the ankle, and which is hidden for the knee).

These oscillations (of varying frequency) generate changes in the measurement provided by the force sensors that are strategically located under the foot. Then, the signals coming from these sensors are amplified and filtered at hardware level, and finally these signals are digitally processed in real time to obtain the ZMP value (see Figure 12). It should be noticed that with this simplified prototype it is only possible to test the proposed robust cascade controller in the sagittal plane, although the results can be translated to the lateral one.

Figure 13 shows a plot with a family of curves of amplitude $|G_{ai}(j\omega)|$ for different values of $\boldsymbol{A}_i$ (signal amplitude) as a function of the frequency ω, for an operation point located at the center of the trunk trajectory. Here, it can be seen that the nominal solid rigid model that suggests a quadratic relationship between $|G_{ai}(j\omega)|$ and ω, does not correspond to the experimental results, because $|G_{ai}(j\omega)|$ only has a quadratic behavior at low frequencies. For frequencies above 2 Hz, it looks like the system model is very much influenced by

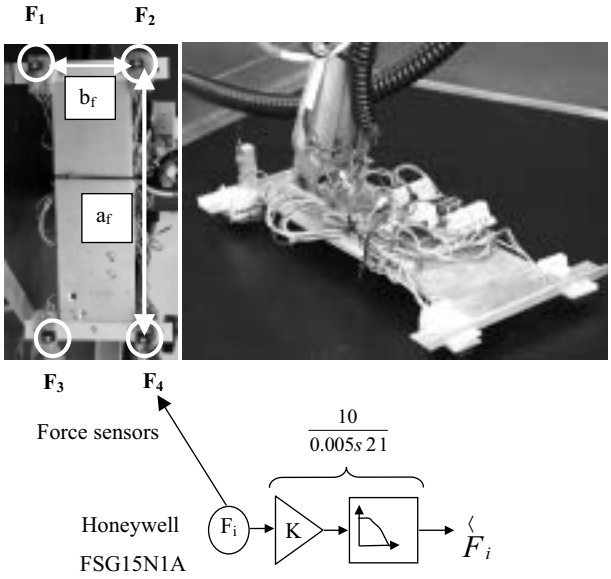

$$ZMP_s \mid \frac{a_f}{2}\frac{(\overleftarrow{F_1} 2 \overleftarrow{F_2}) 4 (\overleftarrow{F_3} 2 \overleftarrow{F_4})}{\overleftarrow{F_1} 2 \overleftarrow{F_2} 2 \overleftarrow{F_3} 2 \overleftarrow{F_4}} \quad \text{Sagittal plane}$$

$$ZMP_l \mid \frac{b_f}{2}\frac{(\overleftarrow{F_2} 2 \overleftarrow{F_4}) 4 (\overleftarrow{F_1} 2 \overleftarrow{F_3})}{\overleftarrow{F_1} 2 \overleftarrow{F_2} 2 \overleftarrow{F_3} 2 \overleftarrow{F_4}} \quad \text{Lateral plane}$$

$a_f = 270$ mm

$b_f = 100$ mm

Fig. 12. Force sensors, amplifiers, filters, and mathematical terms for ZMP calculation.

the mechanical structure oscillatory modes, and also by some nonlinear effects originated in the actuator. In addition, if a similar analysis is performed for the phase $\angle G_{ai}(j\omega)$ at the same operating point (see Figure 14), it can be verified that the phase of the curve family $\angle G_{ai}(j\omega)$ does not correspond to the nominal solid rigid model phase that should be constant.

For the nominal model of the ZMP transfer function a rigid solid model is chosen as $G_P(j\omega) = G_P(s) = c_3 s^2 - c_0$. To calculate the coefficients c_3 and c_0 a correlation between the different families $G_{ai}(j\omega)$ and $G_P(j\omega)$ by means of a weighted least-squares method in the interval $0.1 \leq \omega \leq 30$ rad s^{-1} is made. However, the resulting model does not correspond to a causal system and, consequently, the rigid solid model is modified by adding four poles located far from the origin (so not affecting significantly such a model inside the defined frequency interval). Doing so,

$$G_P(j\omega) = G_P(s) = \frac{p_4 p_3 p_2 p_1 (c_3 s^2 - c_0)}{(s + p_4)(s + p_3)(s + p_2)(s + p_1)}.$$

By choosing as the operating point the center of the SMART mechanical transmission (flat section of Figure 1), the experimental results shown in Figures 13 and 14 were obtained. For this operating point, the following transfer function has been selected:

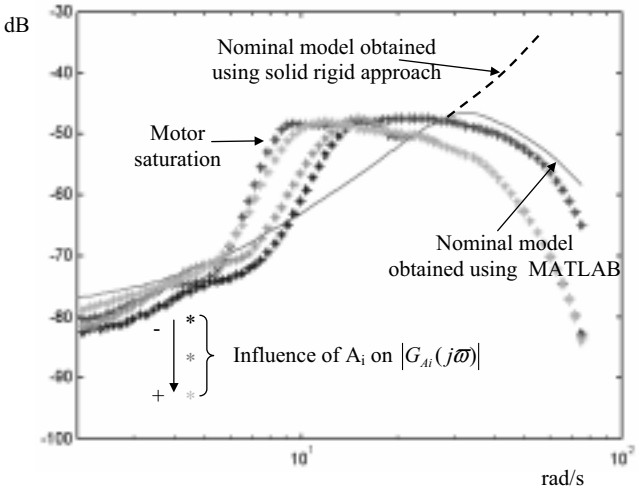

Fig. 13. $|G_{Ai}(j\omega)|$ versus ω for the central operating point.

$$G_P(j\omega) = G_P(s) = \frac{7.1s^2 - 144.1}{s^4 + 86.2s^3 + 3718s^2 + 93908s + 1.185 \times 10^6}. \quad (9)$$

In order to determine the weighting function, $W_G(j\omega)$, it suffices to find a stable and minimum phase function such that

$$|W_G(j\omega)| \geq \left| \frac{G_{Ai}(j\omega)}{G_P(j\omega)} - 1 \right|,$$

for any value of A_i and ω.

Thus, a weighting function $W_G(j\omega)$ can be obtained, which bounds the model uncertainty and the different curve families $G_{Ai}(j\omega)$ reflecting the nonlinear effects. Moreover, it can be demonstrated (Caballero 2002; see Figure 15) that it is appropriated to select

$$W_G(j\omega) = W_G(s) = \frac{14.8s^4 + 121.6s^3 + 498.9s^2 + 1199.0s + 1441.0}{s^4 + 18.3s^3 + 167.3s^2 + 896.3s + 2401.0}. \quad (10)$$

7.2. Linear Robust Control Synthesis

The closed-loop system model, taking into consideration the multiplicative uncertainty, is shown in Figure 16. Now, the goal is to find a controller $C(s)$ that minimizes the following transfer functions.

1. Transfer function between the ZMP_d set point and the error e. This will permit us to minimize the tracking error.

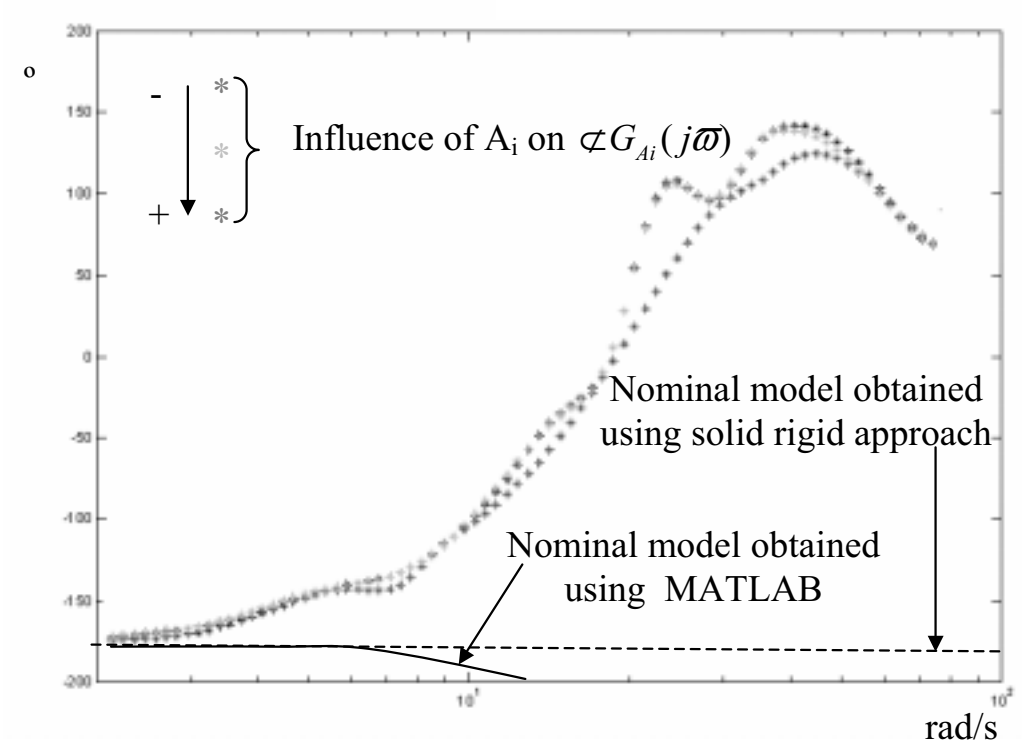

Fig. 14. $\angle G_{Ai}(j\omega)$ versus ω for the central operating point.

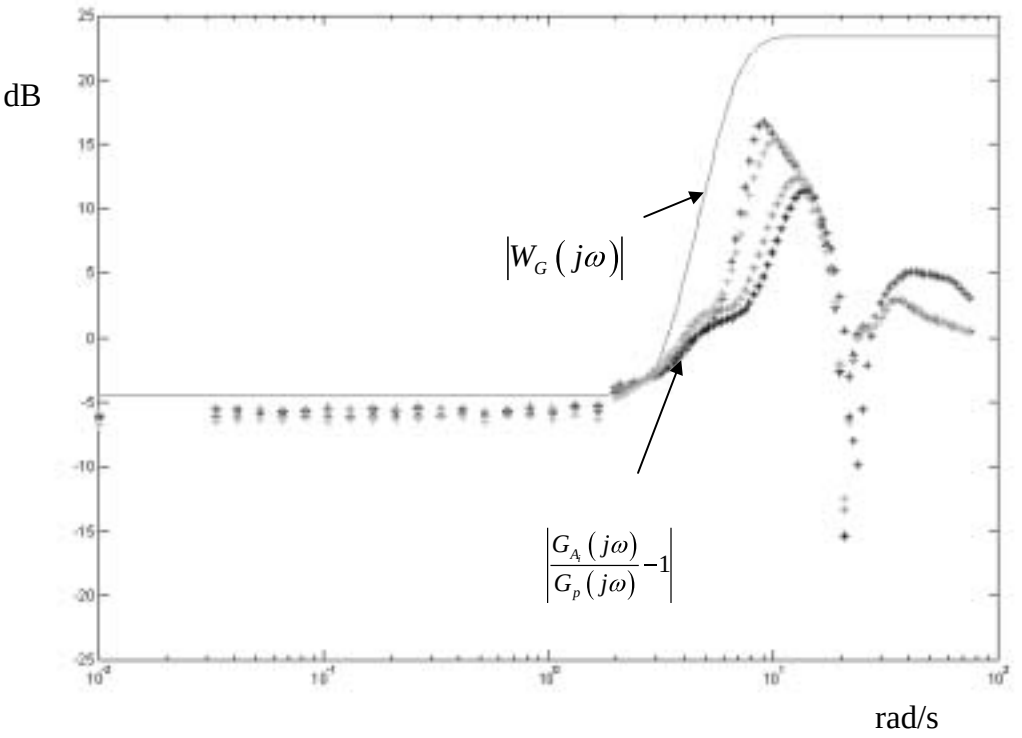

Fig. 15. Weighting function $W_G(j\omega)$ determination.

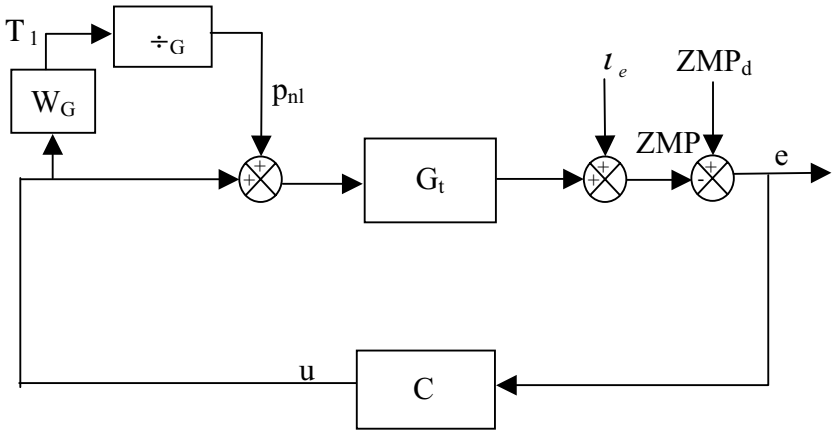

Fig. 16. Closed-loop model taking into account system uncertainty.

2. Transfer function between disturbance δ_e and the ZMP output. This will permit us to attenuate the disturbances.

3. Transfer function between input p_{nl} and output Ω_1. Thus, it will be possible to obtain robustness against model uncertainty.

4. Transfer function between ZMP_d set point and the control output signal. This will permit us to minimize the influence of actuator saturation.

In order to synthesize a controller $C(s)$ with the aforementioned characteristics we can use, for example, the μ Analysis and Synthesis Toolbox from MATLAB, which allows us to design $\mathcal{H}_\infty$ robust controllers. However, before continuing in this direction it is necessary to scale the transfer function $G_P(j\omega)$, to define a weighting function to put some penalty on the control signal saturation, and to define another weighting function $W_P(j\omega)$ to help in specifying a desired closed-loop system performance.

7.2.1. Transfer Function Scaling and Saturation Weighting Function

It is very much recommended to scale the $G_P(j\omega)$ transfer function in order to facilitate the controller design. However, the weighting function $W_G(j\omega)$, which takes into consideration the uncertainty, does not need to be scaled, because of its non-dimensionality. So, the scaled function for $G_P(j\omega)$ can be written as

$$G_{Pe}(s) = \frac{Du}{De} G_P(s)$$

or, in our case,

$$G_{Pe}(s) = \frac{740}{0.27} G_P(s) = \frac{(2.75 \times 10^3)(7.1s^2 - 144.1)}{s^4 + 86.2s^3 + 3718s^2 + 93908s + 1.185 \times 10^6}. \quad (11)$$

One way to avoid the saturation on the control signal at the regulator output is by defining another weighting function. Most authors suggest using

$$0.1 \leq W_u \leq 0.5$$

and, in our particular case, we have selected

$$W_u = 0.15. \quad (12)$$

7.2.2. Performance Weighting Function

The aim of this weighting function is to provide a means to introduce parameters that could influence very positively the closed-loop system characteristics. In this way it will be possible to establish the admitted deviation from the steady-state error, the maximum transient overshoot, and the system bandwidth. Generally, this function can be written as

$$W_P(j\omega) = W_P(s) = \frac{\frac{1}{\mathsf{M}_t} s + \omega_{bx}}{s + \mathsf{A}_t \omega_{bx}}.$$

In our case the following selection has been made:

$\mathsf{M}_t = 2.0$, this parameter influences the maximum overshoot;

$\mathsf{A}_t = 1/200$, this parameter influences the steady-state error;

$\omega_{bx} = 4.0$, this parameter influences the closed-loop system bandwidth.

So, finally, we have obtained

$$W_P(j\omega) = W_P(s) = \frac{0.5s + 4}{s + 0.02}. \tag{13}$$

7.2.3. $\mathcal{H}_\infty$ Controller Synthesis

Once the scaled and the weighting transfer functions have been obtained, then it is possible to update the model presented earlier in Figure 16 by the new model shown in Figure 17. The latter exhibits the interconnected HIMAT (MATLAB) structure, where the variable and the transfer functions are substituted by their scaled equivalents, and where, moreover, the new weighting functions are present.

It can be demonstrated that the four previously mentioned objectives are fulfilled if it is possible to find a controller, $C_e(s)$, such that the following cost function is minimized

$$\min \|\mathsf{N}(C_e)\|_\infty = \|[W_G T_{Pe} \;\; W_P S_{Pe} \;\; W_u C_e S_{Pe}]\|_\infty \tag{14}$$

where

$$S_{Pe} = \frac{1}{1 + G_{Pe} C_{Pe}}$$

and

$$T_{Pe} = \frac{G_{Pe} C_{Pe}}{1 + G_{Pe} C_{Pe}}.$$

This results in a robust controller with the following transfer function:

$$C(s) = K_c \frac{N(s)}{D(s)} \tag{15}$$

where

$$K_c = -4.015;$$

$$N(s) = (s + 8.35)(s + 6.47 + j2.68)(s + 6.47 - j2.68)$$
$$(s + 2.68 + j6.47)(s + 2.68 - j6.47)(s + 23.2)$$
$$(s - 13.0)(s + 47.9)$$

and

$$D(s) = (s + 0.02)(s + 3.8 + j1.1)(s + 3.8 - j1.1)$$
$$(s + 1.6 + j4.0)(s + 1.6 - j4.0)(s + 6.6 + j4.6)$$
$$(s + 6.6 - j4.6)(s + 101 + j101)(s + 101 - j101)$$

However, the controller given by eq. (15) is of ninth order, and it could be too intricate for real-time implementation. So, we suggest proceeding to an order reduction. One appropriated method could be the stochastic balanced truncation (Mustafa and Glover 1981; Desai and Pal 1984; Green 1988; Anderson and Liu 1989; Liu and Anderson 1990). Doing so, a new, sixth-order controller is given by

$$C_{red}(s) = K_{red} \frac{N_{red}(s)}{s D_{red}(s)} \tag{16}$$

where

$$K_{red} = -4.015;$$

$$N_{red}(s) = (s + 2.98 + j6.24)(s + 2.98 - j6.24)(s + 30.0)$$
$$(s - 13.0)(s + 42.4) \text{ and}$$

$$D_{red}(s) = (s + 2.94)(s + 1.47 + j3.96)(s + 1.47 - j3.96)$$
$$(s + 100.3 + j100.3)(s + 100.3 - j100.3)$$

Figure 18 shows a comparison of the frequency response between the reduced-order controller and the full-order controller. It can be noticed that the differences are very small. Nevertheless, Figure 19 shows a frequency domain comparison using the Nyquist diagram for different families of transfer functions (taken from many other experiments), and it can be verified that there is no significant much better behavior when using the suboptimal full-order solution than when using the reduced-order solution.

Another interesting point is to open the possibility of using, for the manipulated output signal from the $\mathcal{H}_\infty$ controller, a speed signal instead of a position signal. In this case, the reference signal that corresponds to the robust controller (VSC) reference speed, can be written as

$$\dot{\gamma}_t(s) = s\gamma_t(s) = C_{red}(s)e(s)$$
$$= K_{red} \frac{N_{red}(s)}{D_{red}(s)} e(s). \tag{17}$$

8. Experimental Evaluation of the Proposed Cascade Robust Controller *VSC*/$\mathcal{H}_\infty$

The proposed robust cascade controller performance can be evaluated injecting the system external disturbances (dynamic external forces). Such disturbances are aimed to emulate the effect on the ZMP that takes place in biped locomotion when changing from double support to single support. Besides, the use of external dynamic forces is also very helpful to predict the robot behavior under sudden terrain changes and small collisions against other tiny bodies during the execution of a normal locomotion gait.

To enter disturbances the experimental setup consists of a one-degree-of-freedom mobile platform and a number of calibrated weights (0.5, 1, and 2 kg). The simplified double-support biped prototype is placed on the platform (Figure 20, right side shows "simplified" robot not showing SMART actuators (illustrated by $q_i = f_i(\gamma_i)$), which can be seen in the photograph for the ankle, and which is hidden for the knee).

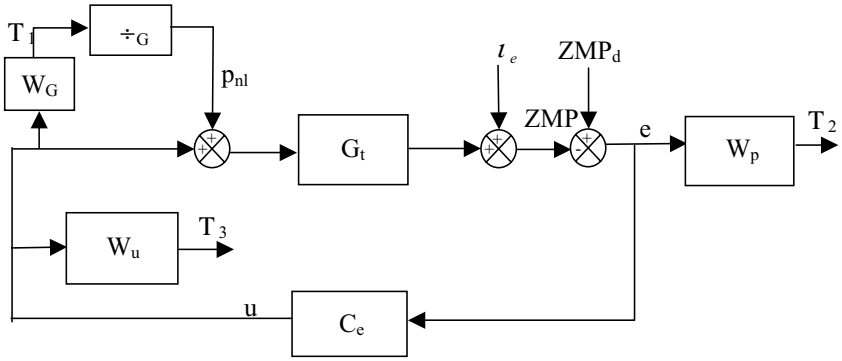

Fig. 17. Mixed sensitivity $\mathcal{H}_\infty$ framework for the outer robust feedback controller design.

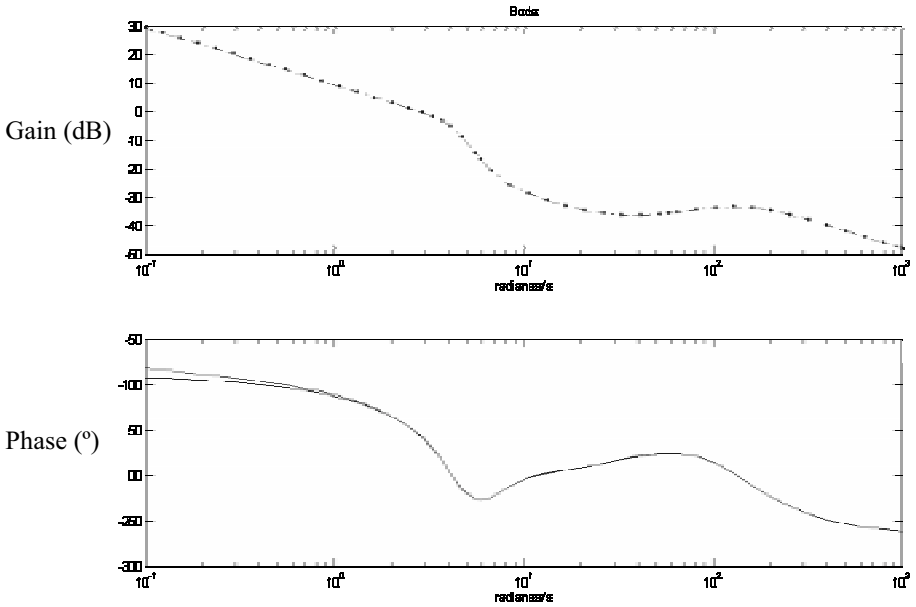

Fig. 18. Robust $\mathcal{H}_\infty$ controller: comparison of full-order and reduced-order models.

SMART actuators have different transmission functions, as illustrated in Figure 20. Experiments are intended to compare the robot response against external disturbances with and without ZMP feedback. The estimated dynamical model is given by

$$\hat{\Psi} \approx 200.25 \left(\begin{bmatrix} \cos\left(\frac{\gamma_1 - 50}{236}\right) & 0 \\ 0 & \cos\left(\frac{\gamma_2 - 270}{236}\right) \end{bmatrix} \begin{bmatrix} 1.0 \times 10^{-6} & 1.7 \times 10^{-6} \\ 1.7 \times 10^{-6} & 3.0 \times 10^{-6} \end{bmatrix} \begin{bmatrix} \cos\left(\frac{\gamma_1 - 50}{236}\right) & 0 \\ 0 & \cos\left(\frac{\gamma_2 - 270}{236}\right) \end{bmatrix} \right) + 200.25 \begin{bmatrix} 2.6 \times 10^{-6} & 0 \\ 0 & 2.6 \times 10^{-6} \end{bmatrix}$$

$$\hat{\Phi} = \begin{bmatrix} 3.9 \times 10^{-2} & 0 \\ 0 & 3.9 \times 10^{-2} \end{bmatrix}$$

$$\hat{\Upsilon} \approx \frac{200.25}{236^2} \begin{bmatrix} \frac{1}{6}\cos\left(\frac{\gamma_1 - 50}{236}\right) & 0 \\ 0 & \frac{1}{2}\cos\left(\frac{\gamma_2 - 270}{236}\right) \end{bmatrix} \begin{bmatrix} 2.93751.2812 \\ 1.28120.5938 \end{bmatrix} \begin{bmatrix} \frac{1}{6}\sin\left(\frac{\gamma_1 - 50}{236}\right) & 0 \\ 0 & \frac{1}{2}\sin\left(\frac{\gamma_2 - 270}{236}\right) \end{bmatrix}$$

$$\hat{\Delta} = -200.25 \begin{bmatrix} \cos\left(\frac{\gamma_1 - 50}{236}\right) & 0 \\ 0 & \cos\left(\frac{\gamma_2 - 270}{236}\right) \end{bmatrix} \begin{bmatrix} 0.1670.167 \\ 0 \quad 0.5 \end{bmatrix} \begin{bmatrix} \left(\frac{20.84}{236}\right)\sin(\theta_1) \\ \left(\frac{13.49}{236}\right)\sin(\theta_2) \end{bmatrix}.$$

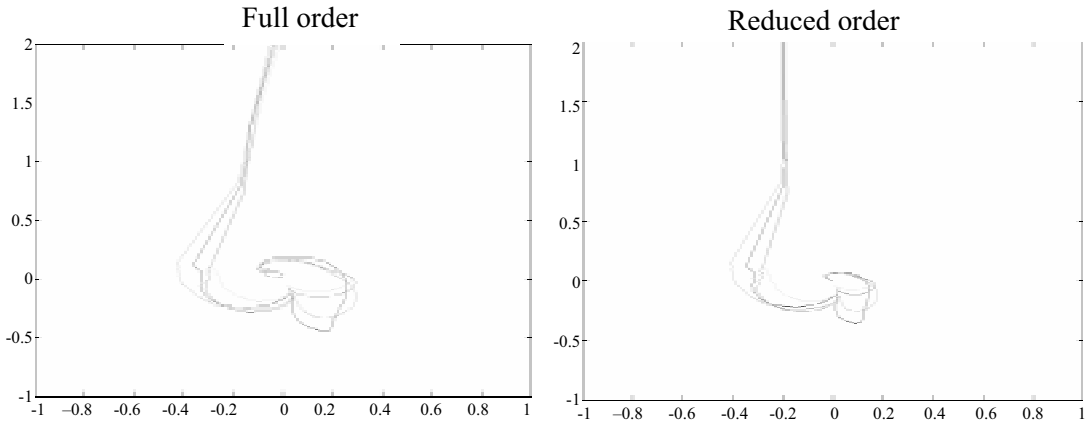

Fig. 19. Nyquist stability analysis for robust $\mathcal{H}_\infty$ controller: full-order (left); reduced-order (right).

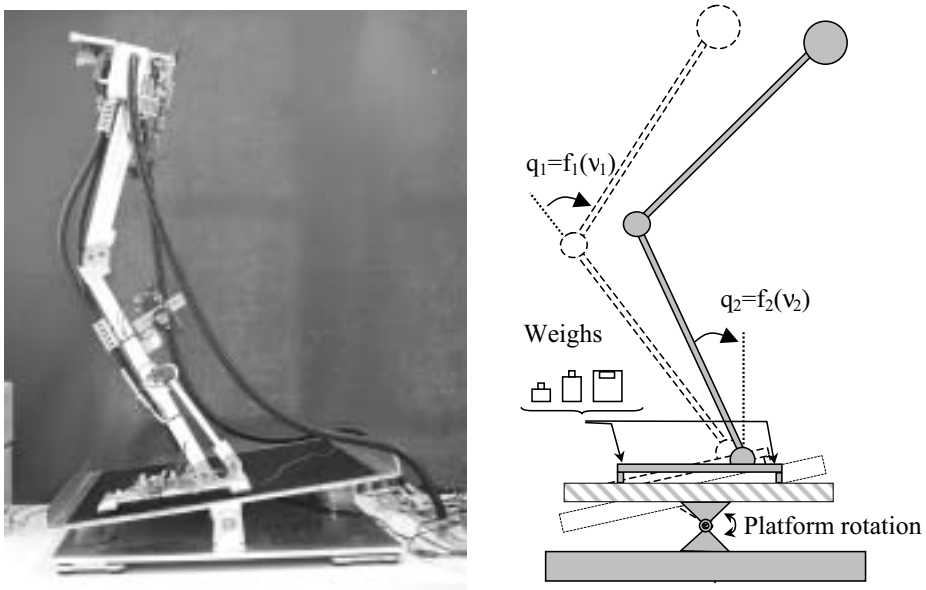

Fig. 20. Experimental setup: two-degrees-of-freedom prototype, mobile platform, and weight units to enter disturbances.

So, we have

$$U = \hat{\Psi}\ddot{\gamma}_r + \hat{\Phi}\dot{\gamma}_r + \hat{\Upsilon}\dot{\gamma}_r^2 + \hat{\Delta} - \hat{E}_{RK}k_l\varphi - \hat{E}_{RK}k_s v(\varphi, \varphi_a).$$

The VSC controller was synthesized using eqs. (5)–(8) with

$$\hat{E}_{RK} = \begin{bmatrix} 0.22 & 0 \\ 0 & 0.22 \end{bmatrix}; \quad k_l = \begin{bmatrix} 37.5 & 0 \\ 0 & 22.5 \end{bmatrix};$$

$$k_s = \begin{bmatrix} 10 & 0 \\ 0 & 10 \end{bmatrix}; \quad s_a = \begin{bmatrix} 2020 \end{bmatrix}^T$$

$$\varphi = \begin{bmatrix} \varphi_1 & \varphi_2 \end{bmatrix}^T = \begin{bmatrix} \lambda_1 e_1 + \dot{e}_1 & \lambda_2 e_2 + \dot{e}_2 \end{bmatrix}^T$$

$$= \begin{bmatrix} 15e_1 + \dot{e}_1 & 25e_2 + \dot{e}_2 \end{bmatrix}^T.$$

A sampling time of 0.9 ms was used. Also, we note here that the experimentally obtained nominal ZMP transfer function was presented previously.

8.1. Step Disturbance Acting on the ZMP

To enter a step disturbance to the ZMP it suffices to place or withdraw single masses on the foot front/rear. This method resembles the situation created on the support leg by the transfer leg in a biped robot. The time response of the open-loop system can be observed in the upper part of Figure 21. Just below (second row of Figure 21) is shown the closed-loop system response for the same disturbances. In both cases it can be seen that the controller has the capability to restore

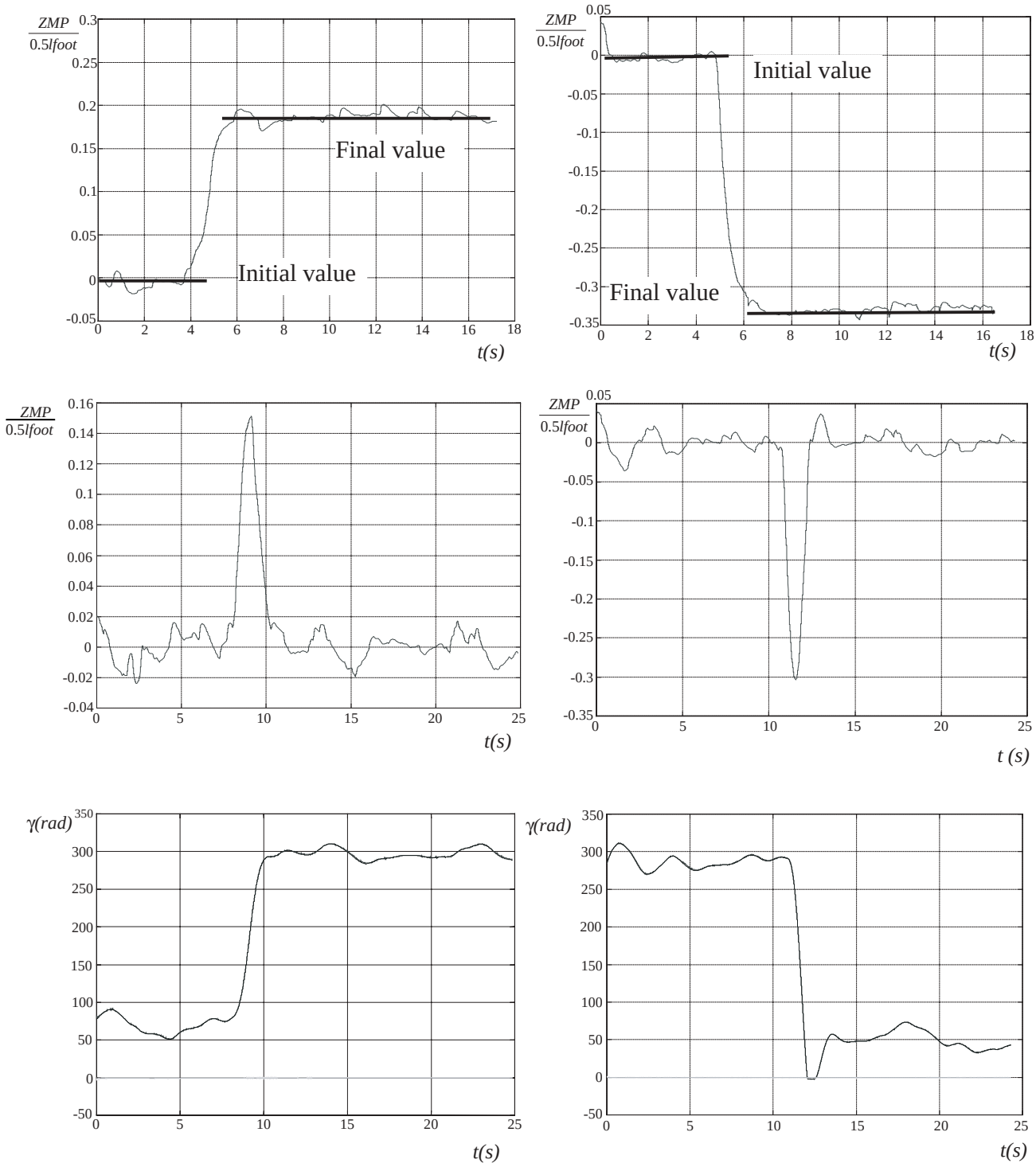

Fig. 21. Step disturbance on the ZMP: comparison of open-loop versus closed-loop behavior.

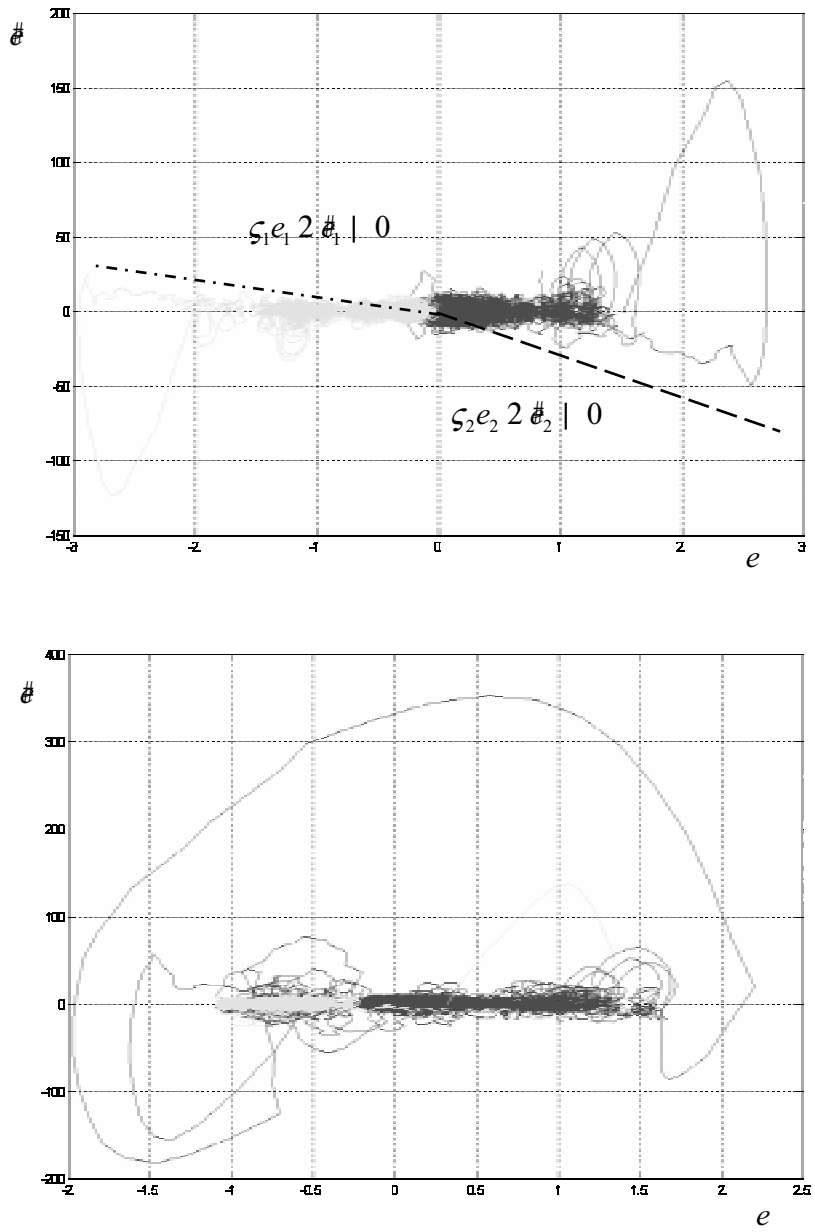

Fig. 22. Dynamic error. Attraction effect exerted by the quasi-sliding planes on the system state variables (trunk (dark) and ankle (bright)): small disturbance (top); large disturbance (bottom).

the reference ZMP value in approximately 2 s. Also, it should be noticed that, in closed loop, the ZMP maximum error is always a lower amount of the value it reaches in open loop. The trunk set point γ_{tr} created by the external $\mathcal{H}_\infty$ controller to stabilize the ZMP and the position time response γ_t of the trunk produced by the internal control loop (VSC) can be seen in the bottom part of Figure 21. The dynamic error behavior is shown in Figure 22, where the attraction effect exerted by the quasi-sliding planes, $\varphi_1 = \lambda_1 e_1 + \dot{e}_1 = 0$ and $\varphi_2 = \lambda_2 e_2 + \dot{e}_2 = 0$, on the system states is noticeable. Also, Figure 22 serves to illustrate that, in the presence of a large disturbance, one of the states escapes from the quasi-sliding region, but it returns very quickly.

8.2. Step Disturbance Acting on the Platform

One step input to the platform does not generate one step disturbance on the robot ZMP value. This sudden change in the platform position originates a more complex disturbance (see Figure 23, left) because of the acceleration effect. Nevertheless, the use of this step disturbance is very remarkable, because it can be used to approximate what happens when the

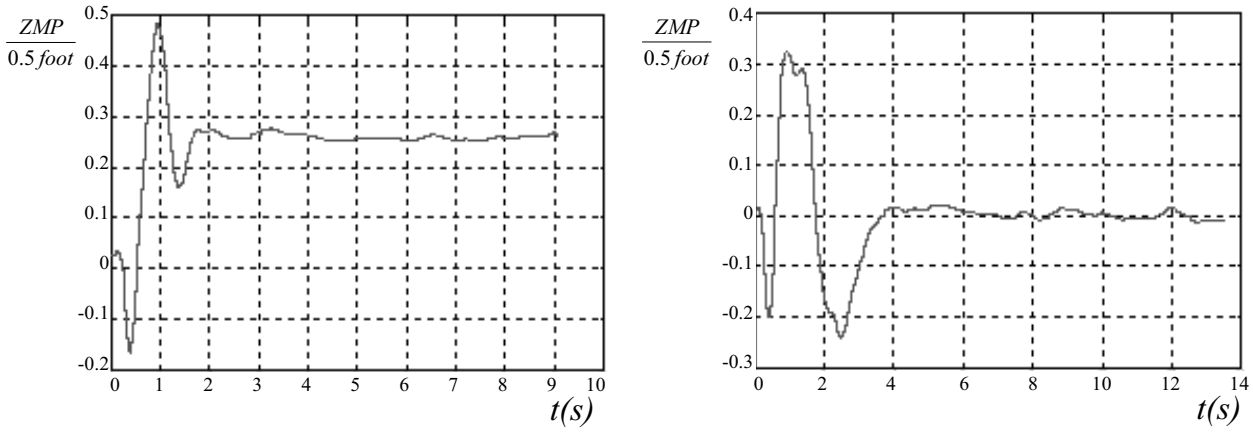

Fig. 23. ZMP dynamic evolution after step input to the platform: without control (left) and with control (right).

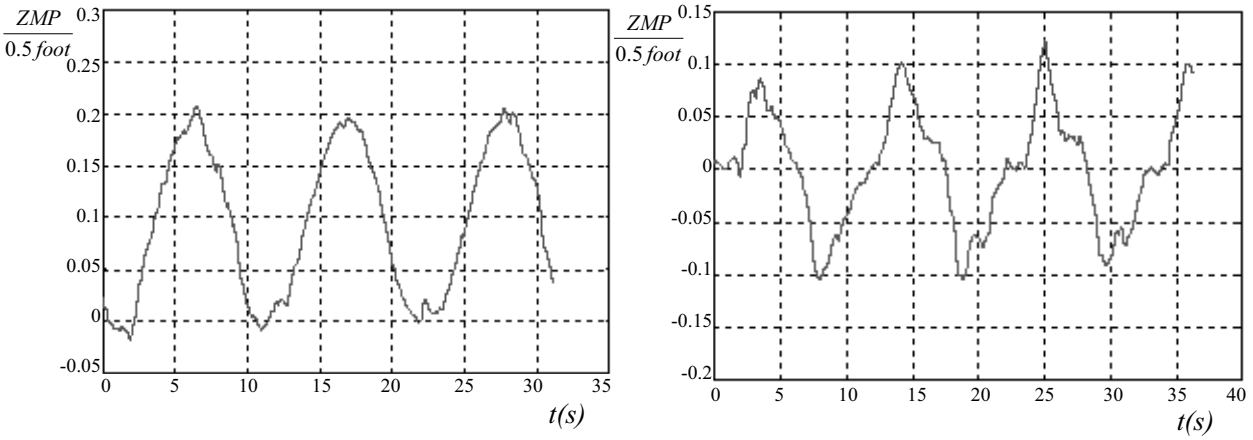

Fig. 24. Robot ZMP trajectories after sinusoidal disturbance acting on the platform: open loop (left) and with closed-loop control (right).

floor slope is unexpectedly changed. The closed-loop system behavior is shown on the right side of Figure 23. It can be noticed that the controller is able to stabilize the robot in about 4 s. The control input for the trunk γ_{tr} and the system outputs regarding the positions for γ_t and q_t and the dynamic error trajectories for the trunk and for the ankle joints are omitted here for the sake of brevity (Caballero 2002).

8.3. Sinusoidal Disturbance Acting on the Platform

Another relevant experiment to test the controller robustness properties consists of analyzing the system response under sinusoidal disturbances. Differently from the step input, a sinusoidal position change on the platform results in a sinusoidal disturbance on the ZMP values. This is mainly due to the fact that the second derivative of a sinusoidal profile in position is also sinusoidal (see the left side of Figure 24). The right side of Figure 24 shows the ZMP time response when the system is under closed-loop control. As can be seen, the controller is only able to stabilize the mean changes of the reference signal. However, this control action is very valuable, because it permits us to maximize the robot ZMP stability margin (before it was 0.2 and now it is 0.1; notice that the ZMP value is normalized to $0.5 l_{foot}$). Many other experiments have shown the system capabilities for trajectory tracking.

8.4. Combined Disturbance Acting on the Platform

To enable further testing of the controller performance, the next step is to subject the system to a combined disturbance action. This has been accomplished by rotating the platform and by placing/withdrawing masses on the foot surface (1 kg). The closed-loop system response under these disturbances is presented in Figure 25. In this case, the ZMP behavior is

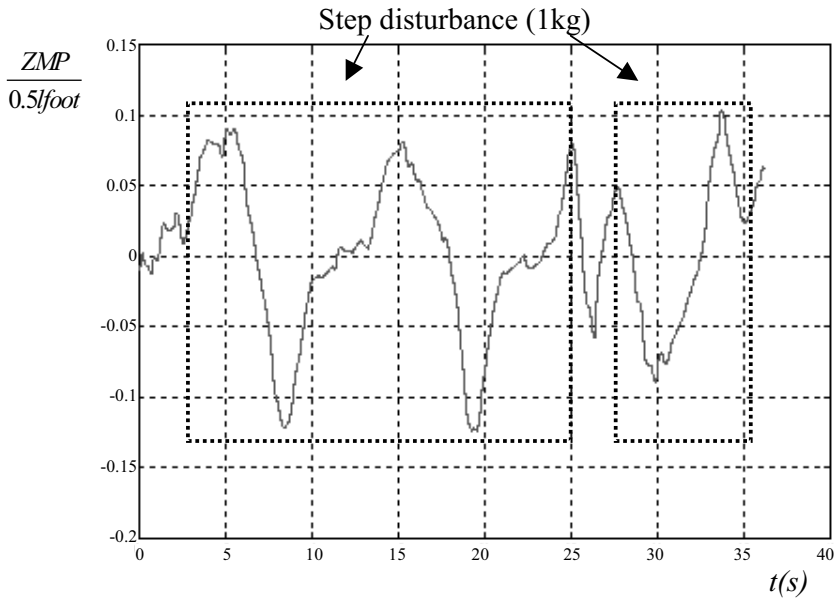

Fig. 25. ZMP closed-loop response after being disturbed with a combination of sinusoidal platform movement and with the placement of masses on the foot.

similar to the case shown before in Figure 24 (left), and, in any case, the stability margin for the ZMP is kept below 0.1.

9. Adding Feedforward Compensation to the $VSC/\mathcal{H}_\infty$ Controller

As shown in the preceding section, the proposed cascade $VSC/\mathcal{H}_\infty$ controller exhibits a fair performance under different disturbances. However, due to the limitations imposed by the non-minimum phase plant characteristics, it is not possible to stabilize the system in less than 2 s. This situation could lead to difficulties when other robot links are also in progress. It has been demonstrated (Pernebo 1981) that the addition of feedforward terms does not affect the stability, because it is determined by the feedback loop. So, it is proposed to incorporate some feedforward terms to the controller, as follows:

$$\dot{\gamma}_{rt}(t) = K_{FF}^T \dot{\gamma}_{rd}(t) + C_{ZMP}(e_{ZMP}(t)).$$

In our experimental setup, the next, simple feedforward action, has been selected:

$$K_{FF}^T = [1.25]$$

$$\dot{\gamma}_{rd}(t) = \dot{\gamma}_{r1}(t).$$

The influence of the added feedforward compensation is investigated as follows. First, the robot stability is disturbed by inputting to the ankle joint a sinusoidal signal (in position). In these conditions it is foreseen that the robot should perform in a similar way to the previous (recall Figure 24) time when a sinusoidal input was applied to the platform. This is confirmed by the results shown in Figure 26 (left), where the controller keeps the ZMP stability margin bounded by 0.1.

After that, the robot is subjected to the same disturbances but the feedforward terms with $K_{FF}^T = [1.25]$ are added. The obtained results are summarized in Figure 26 (right), and it can be seen that the new controller structure has been able to substantially improve the stability margin up to a value of 0.04, i.e., the stability margin has been improved 2.5 times (note that the y-axis scales are different).

10. Final Remarks on the $VSC/\mathcal{H}_\infty$ Controller Performance

The presented experimental results concerning the cascade robot controller $VSC/\mathcal{H}_\infty$ are limited to one operating point, which in this case has been selected at the center of the near-flat area of the SMART transmission (Figure 1).

However, the synthesized regulator about such operating point has demonstrated a very good behavior along all the near-flat SMART area. For the other areas located outside this region, another regulator, synthesized in similar way, can be employed (Figure 27). Such a configuration, where the outer loop regulator is commuting between $C_{red\_C}(s)$ and $C_{red\_E}(s)$ depending on the operation region, has been demonstrated to be very reliable in practice (Caballero 2002).

11. Conclusions

We have presented an integrated biped robot dynamical model including the effect of nonlinear actuators and the ZMP. This

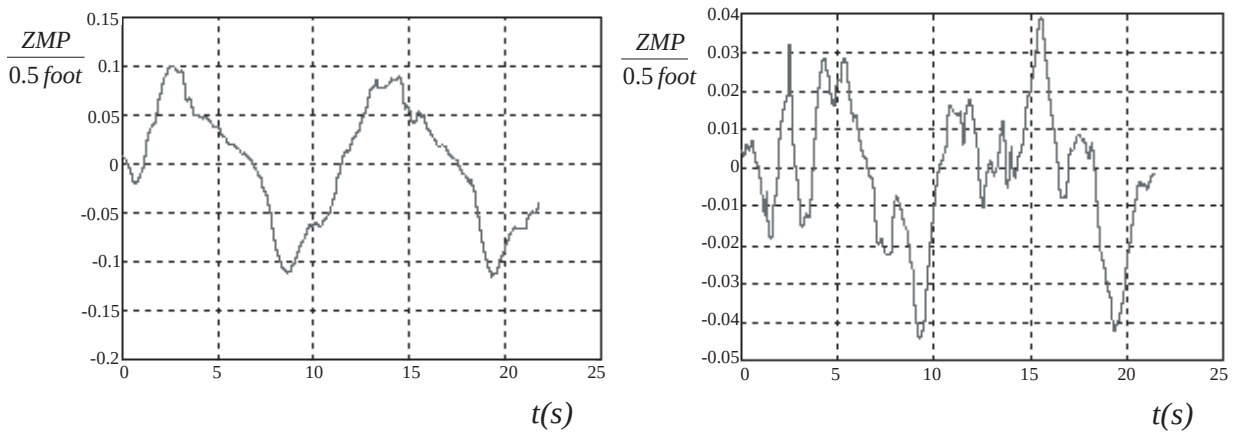

Fig. 26. ZMP behavior after being disturbed with a sinusoidal input in the ankle joint: without feedforward term (left); with feedforward term (right).

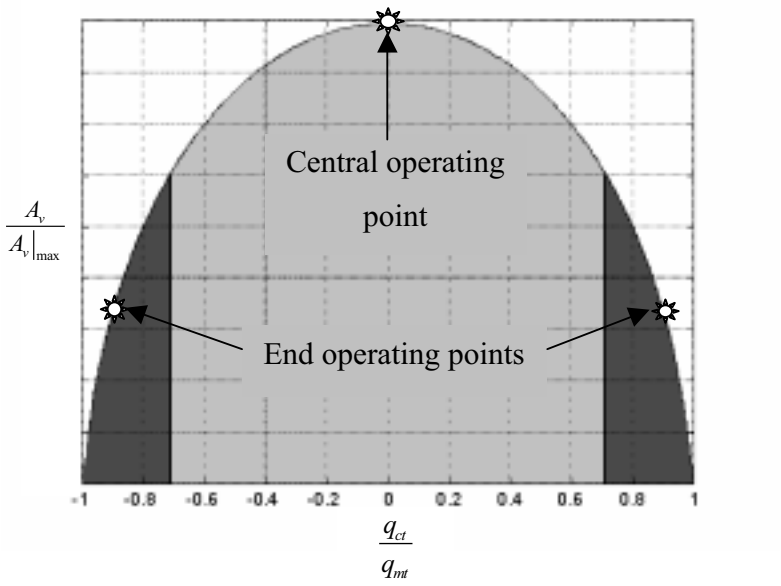

Regulator $C_{red\_C}(s) = K_{red\_C}\frac{N_{red\_C}(s)}{sD_{red\_C}(s)}$

$K_{red\_C} = 44.015;\ N_{red\_C}(s) = (s+2.98)(s+6.24j)(s+2.98-6.24j)(s+30.0)(s+13.0)(s+42.4)$

$D_{red\_C}(s) = s(s+2.94)(s+1.473.96j)(s+1.473.96j)(s+100.3100.3j)(s+100.3100.3j)$

Regulator $C_{red\_E}(s) = K_{red\_E}\frac{N_{red\_E}(s)}{sD_{red\_E}(s)}$

$K_{red\_E} = 27.46;\ N_{red\_E}(s) = (s+7.5331.70j)(s+7.5331.70j)(s+1.0+3.59j)(s+1.0-3.59j)(s+0.49)$

$D_{red\_E}(s) = s(s+0.38)(s+1.871.58j)(s+1.871.58j)(s+65.469.80j)(s+65.469.80j)$

Fig. 27. Operating regions for the outer feedback loop $VSC/\mathcal{H}_\infty$ regulators.

model was used to establish a relationship between the robot state variables and the stability margin of the foot contact surface and the supporting ground. To ensure this contact, the ZMP was measured and used in a direct, stabilizing, feedback loop. A $VSC/\mathcal{H}_\infty$ robust cascade control architecture has been demonstrated to be a correct approach to cope with the nonlinear system characteristics and with its associated uncertainties.

On the other hand, frequency domain techniques have proven to be very effective to obtain and to validate experimentally the transfer function between the robot joint variables and the ZMP with its associated uncertainty in the presence of nonlinearities.

The performed experiments using a simplified prototype have allowed us to evaluate the proposed cascade controller $VSC/\mathcal{H}_\infty$ that has been able to keep the robot joint positioning set points and to stabilize the ZMP reference (desired) position against different external disturbances. However, due to the inherent limitations owing to the non-minimum phase properties of the physical system, the achieved speed of response is slow. To solve this problem, the use of a feedforward term in the outer loop controller has proved to be very effective for substantially improving the stability margin. Other performed experiments with step disturbances have revealed that the time response is also improved.

Acknowledgments

The authors would like to acknowledge funding from Consejería de Educación y Cultura of Comunidad de Madrid, under research projects 07T/0040/1998 and 07T/0022/2001, and the financial support from the Ministry of Science and Technology of Spain (Project "Theory of optimal dual drives for automation and robotics"). The EC funded CLAWAR Thematic Networks (BET2-546 and G1RT-CT-2002-05080) has been very supportive of all our activities carried out regarding climbing and walking robots.

References

Akinfiev, T. 1996. The resonance drives with adaptive control. *Proceedings of the 11th ASCE Engineering Mechanics Conference*, New York, pp. 947–950.

Akinfiev T., Armada M., and Caballero R. 2000. Actuador para las piernas de un robot caminante. Patent Number ES 2 166 735 A1.

Anderson, B., and Liu, Y. 1989. Controller reduction: concepts and approaches. *IEEE Transactions on Automatic Control* 34(8).

Armada, M., Caballero, R., Akinfiev, T., Montes, H., Manzano, C., Pedraza, L., Ros, R., and Gonzalez de Santos, P. 2002. Design of SILO2 Humanoid Robot. *Proceedings of the IARP International Workshop on Humanoid and Friendly Robots*, Tsukuba, Japan.

Armada, M., Caballero, R., Akinfiev, T., Montes, H., and Pedraza, L. 2003a. Extending humanoid robot functioning by proficient application of nonlinear actuators. *Proceedings of the 11th International Conference on Advanced Robotics*, Coimbra, Portugal, pp. 1757–1762.

Armada, M., González de Santos, P., Jiménez, M.A., and Prieto, M. 2003b. Application of CLAWAR machines. *International Journal of Robotics Research* 22(3–4):251–264.

Caballero, R. 2002. Control de robots bipedos con accionamientos no lineales. PhD Thesis, Politecnic University of Madrid, Spain.

Caballero R., Akinfiev T., Montes H., and Armada M. 2001. On the modelling of SMART nonlinear actuator for walking robots. *Proceedings of the 4th International Conference on Climbing and Walking Robots*, Karlsruhe, Germany, pp. 24–26.

Caballero R., Akinfiev T., Montes H., Manzano C., and Armada M. 2002a. Design of the SMART actuated ROBICAM biped robot. *Proceedings of the 5th International Conference on Climbing and Walking Robots*, Paris, France, pp. 409–416.

Caballero, R., Akinfiev, T., and Armada, M. 2002b. Robust cascade controller for Robicam biped robot: preliminary experiments. *Proceedings of the 5th International Conference on Climbing and Walking Robots*, Paris, France, pp. 147–154.

Desai, U., and Pal, D. 1984. A transformation to stochastic model reduction. *IEEE Transactions on Automatic Control* 29(12):1097–1100.

Eldukhri, E. 1996. Design and Control of a Biped Walking Robot. PhD Thesis, Department of Electronic and Electrical Engineering, University of Salford, UK.

Fujimoto, Y., Obata, S., and Kawamura, A. 1998. Robust biped walking with active interaction control between foot and ground. *Proceedings of the 1998 IEEE International Conference on Robotics and Automation (ICRA)*, Leuven, Belgium.

Furushu, J., and Masubushi, M. 1986. Control of a dynamical biped locomotion system for steady walking. *Journal of Dynamic Systems, Measurement and Control* 108(6):111–118.

Furushu, J., and Sano, A. 1990. Sensor-based control of a nine-link biped. *International Journal of Robotic Research* 9(2):83–89.

Gienger, M., Loffler, K., and Pfeiffer, F. 1999. Design and control of a biped walking and jogging robot. *Proceedings of the 2nd International Conference on Climbing and Walking Robots*, Portsmouth, UK, pp. 48–58.

González de Santos, P., Armada, M., and Jiménez, M.A. 2000. Ship building with ROWER. *IEEE Robotics and Automation Magazine* 7(4):35–43.

Goswami, A. 1999. Postural stability of biped robots and the foot-rotation indicator (FRI) point. *International Journal of Robotics Research* 18(6):523–533.

Green, M. 1988. A relative error bound for stochastic

truncation. *IEEE Transactions on Automatic Control* 33(10):961–965.

Hemami, H. 1978. Reduced-order models for biped locomotion. *IEEE Transactions on Systems, Man, and Cybernetics* 8(4):321–325.

Hemami, H., Weimer, F., and Koozekanani, S. 1973. Some aspects of the inverted pendulum problem for modeling of locomotion systems. *IEEE Transactions on Automatic Control*, pp. 658–661.

Hirai, K., Hirose, M., Haikawa, Y., and Takenaka, T. 1998. The Development of Honda Humanoid Robot. *Proceedings of the IEEE International Conference on Robotics and Automation.* Leuven, Belgium, pp. 1321–1326.

Hirai, K. 1999. The Honda humanoid robot: development and future perspective. *Industrial Robot* 26(4):260–266.

Hirosi, G., Tomharu, K., Masato, H., and Masao, N. 1991. Articulated structure for legged walking robot. Patent Number EP 0433096.

Liu, Y., and Anderson, B. 1990. Frequency weighted controller reduction methods and loop transfer recovery. *Automatica* 26(3):487–497.

McGeer, T. 1990. Passive dynamic walking. *International Journal of Robotic Research* 9(2):62–81.

Medrano-Cerda, G., and Eldukhri, E. 1997. Biped robot locomotion in sagittal plane. *Transactions on Instrument Measurement and Control* 19(1):38–49.

Mennitto, G., and Buehler, M. 1997. LADD transmissions: design, manufacture, and new compliance models. *ASME Journal of Mechanical Design* 119(2):197–203.

Mita, T, Yamagushi, T., Kashiwase, T., and Kawase, T. 1984. Realization of a high-speed biped using modern control theory. *International Journal of Control* 40(1):107–119.

Montes, H., Pedraza, L., Armada, M., Akinfiev, T., and Caballero, R. 2004. Adding extra sensitivity to SMART nonlinear actuator using sensor fusion. *Industrial Robot* 31(2):179–188.

Mustafa, D., and Glover, K. 1991. Controller reduction by H_∞ balanced truncation. *IEEE Transactions on Automatic Control* 36(6):668–682.

Pernebo, L. 1981. An algebraic theory for the design of controllers for linear multivariable systems: part I and part II. *IEEE Transactions on Automatic Control* 26(1):171–182, 183–194.

Pfeiffer, F., Löffler, K., and Gienger, M. 2000. Design aspects of walking machines. *Proceedings of the 3rd International Conference on Climbing and Walking Robots*, Madrid, Spain, pp. 17–38.

Pratt, J., Dilworth, P., and Pratt, G. 1977. Virtual model control of a bipedal walking robot. *Proceedings of the International Conference on Robotics and Automation (ICRA)*, Albuquerque, NM.

Raibert, M., Tzafestas, S., and Tzafestas, C. 1993. Comparative simulation study of three control techniques applied to a biped robot. *Proceedings of the IEEE International Conference on Systems, Man and Cybernetics*, Le Touquet, France, Vol. 1, pp. 494–502.

Sardin, P., Rostami, M., and Besonet, G. 1998. An anthropomorphic biped robot: dynamic concepts and technological design. *IEEE Transactions on Systems, Man and Cybernetics: Part A* 28(6).

Seo, Y., and Yon, Y. 1995. Design of a robust dynamic gait of the biped using the concept of dynamic stability margin. *Robotica* 13:461–468.

Sias, F., and Zheng, Y. 1987. Static stability problems in biped robot design. *Proceedings of the 19th South-Eastern Symposium on System Theory*, Clemson, SC.

Skogestad, S., and Postlethwaite, I. 1996. *Multivariable Feedback Control*, Wiley, Chichester.

Takanishi, A., Tochizawa, M., Taraki, H., and Kato, I. 1989. Realization of dynamic biped walking stabilized with trunk motion under known external force. *Proceedings of the International Conference on Advanced Robotics*, Ohio, USA.

Tzafestas, S., Krikochoritis, T., and Tzafestas, C. 1997. Robust sliding mode control of nine-link biped robot walking. *Journal of Intelligent and Robotic Systems* 20:375–402.

Van de Straete, H., and Schutter, J. 1999. Optimal time varying transmission for servo motor drives. *Proceedings of the 10th World Congress on Theory of Machines and Mechanisms*, Oulu, Finland, Vol. 5, pp. 2055–2062.

Vukobratovic, M., and Borovac, B. 2004. Zero moment point—thirty-five years of its life. *International Journal of Humanoid Robotics* 1(1):157–173.

Vukobratovic, M., and Juricic, D. 1968. Contribution to the synthesis of biped gait. *Proceedings of the IFAC Symposium on the Technical and Biological Problems of Control*, Erevan, USSR.

Vukobratovic, M., and Juricic, D. 1969. Contribution to the synthesis of biped gait. *IEEE Transactions on Bio-Medical Engineering* 16(1):1–6.

Vukobratovic, M., and Stokic, D. 1975. Dynamic control of unstable locomotion robots. *Mathematical Biosciences* 24:129–157.

Vukobratovic, M., Borovac, B., Surla, D., and Stokic, D. 1990. *Biped Locomotion*, Springer-Verlag, Berlin.

Waldron, K.J. 2000. From walking to galloping. *Proceedings of the 3rd International Conference on Climbing and Walking Robots*, Madrid, Spain, pp. 1–5.

Winter, D.A. 1990. *Biomechanics and Motor Control of Human Movement*, Wiley, New York.

Yamaguchi, J., and Takanishi, A. 1997. Development of a biped walking robot having antagonistic driven joints using nonlinear spring mechanism. *Proceedings of the IEEE International Conference on Robotics and Automation (ICRA)*, Albuquerque, NM.

Yamaguchi, J., Takanishi, A., and Kato, I. 1993. Development of a biped walking robot compensating for three-axis moment by trunk motion. *Proceedings of the IEEE/RSJ International Conference on Intelligent Robots and Systems (IROS)*, Yokohama, Japan.